Materials Today Physics 36 (2023) 101152

Contents lists available at ScienceDirect

Materials Today Physics

journal homepage: www.journals.elsevier.com/materials-today-physics

Preference for a pressure-induced 3D structure after 1T-$HfSe_2$

Katerina P. Hilleke [a], Ruth Franco [b], Pilar Pertierra [b], Miguel A. Salvadó [b], Eva Zurek [a], J. Manuel Recio [a,b,*]

[a] Department of Chemistry, State University of New York at Buffalo, Buffalo, NY, 14260-3000, United States
[b] MALTA-Consolider Team and Departamento de Química Física y Analítica, Universidad de Oviedo, Av. Julián Clavería 8, E-33006, Oviedo, Spain

ARTICLE INFO

Keywords:
HfSe2
High-pressure
Crystal structure prediction
Phase transition
First-principles calculations
Raman frequencies

ABSTRACT

Extensive crystal structure prediction searches provide evidence of two 3D structures with orthorhombic (*Immm*) and monoclinic (*C2/m*) space groups as reasonable candidates for the first pressure-induced phase of 1T-$HfSe_2$. Our candidates are compared with two recent proposals that keep the 2D nature of the ambient conditions phase and display hexagonal ($P6_3/mmc$) and monoclinic (*C2/m)* symmetry, although the latter has a different structure than our proposed *C2/m* phase. Both of these 2D-like structures are discarded based on simple thermodynamic and kinetic arguments that can be extended to explain the pressure-induced polymorphic sequence of other transition metal dichalcogenides. The computed observables of our orthorhombic phase are fully consistent with the experimental structural and Raman data observed at low and high-pressure.

1. Introduction

Laminar transition metal dichalcogenide (TMD) crystalline compounds show a very rich polytypism due to the presence of simultaneous intralayer covalent bonds and interlayer chalcogenide-chalcogenide weak van der Waals interactions. The variety of possible stacking orders with different layer displacements leads to the existence of a number of stable and metastable polymorphs [1]. As pressure is applied, the interlayer interactions become stronger while the intralayer ones weaken, resulting in a complicated potential energy landscape with many local minima, and the difficulty in finding the symmetry of new emerging polymorphs increases. This difficulty poses a challenge to understanding the crucial role that TMDs play as electronic and optoelectronic components [2], surfactants [3], catalysts [4], or high performance thermoelectric devices [5] in a variety of industrial applications.

For the purpose of this contribution, we specifically highlight the great interest that exists in the necessary determination of the pressure-induced polymorphic sequence of TMDs. Besides the obvious link between structure and function, such studies help understand and anticipate how the electronic behavior in this family of compounds changes as pressure is applied. This is done, in part, by following the evolution of structural data and Raman frequencies with pressure. In the particular case of the semiconductor hafnium selenide, there is a consensus that the emergence of (semi)metallization and superconductivity at high-pressure is connected with the loss of stability of the phases involved in the corresponding pressure-induced transformations [6–9]. This consensus is in agreement with a 'universal phase diagram' suggested by Joe et al. [10] that is able to explain the emergence of superconductivity from a fluctuation of a coexisting phase displaying a charge density wave transition. However, the identification of high-pressure $HfSe_2$ polymorphs remains controversial.

In a recent breakthrough investigation, Rahman et al. [9] proposed a transition to a hexagonal $P6_3/mmc$ structure when pressure is exerted on the 1T-$HfSe_2$ polymorph (with space group $P\,\bar{3}\,m1$), which is the stable phase at atmospheric conditions. The onset of the transition is detected around 16–18 GPa, but this phase coexists with the low-pressure (LP) 1T ($P\,\bar{3}\,m1$) phase up to 24 GPa. Although the hexagonal structure might be an *a priori* plausible high-pressure (HP) candidate, we have found reasonable arguments and computational evidence indicating that 1T-$HfSe_2$ might prefer to transform under pressure into either an orthorhombic or a monoclinic structure with *Immm* and *C2/m* space groups, respectively.

The *C2/m* structure proposed here is distinct from another one with the same symmetry recently proposed by Tian et al. [8], which we will label as *C2/m*-T (for Tian) to avoid confusion. Tian et al. combine exhaustive X-ray diffraction (XRD), Raman, electrical, and magnetic experiments along with theoretical calculations performed using the density functional theory (DFT) approximation in their search for a

* Corresponding author.
E-mail address: jmrecio@uniovi.es (J.M. Recio).

https://doi.org/10.1016/j.mtphys.2023.101152
Received 3 April 2023; Received in revised form 12 June 2023; Accepted 16 June 2023
Available online 19 June 2023

plausible high-pressure candidate of $HfSe_2$. The starting geometry of this polymorph (before optimization) is based on a monoclinic high-pressure structure of VSe_2, which is nevertheless difficult to differentiate experimentally from the ambient condition-1T polytype [11]. As a consequence, the resulting monoclinic structure retains the 2D layered nature of the trigonal phase, in contrast to our candidate and indeed the claims of Tian et al. [8]. The large hysteresis accompanying the transition and high bulk modulus of the phase following 1T-$HfSe_2$ are hallmarks of a 3D structure, incompatible with the layered nature of the *C*2/*m*-T candidate structure. Understanding the dimensionality of the structures comprising the polymorphic sequence of the TMD family will be a key factor discussed later in more detail.

To complete the list of recent experimental investigations of 1T-$HfSe_2$ under hydrostatic pressure, we provide the phase transitions reported by Zhang et al. using synchrotron XRD, Raman, IR reflectivity, and resistance measurements [7]. These authors have also found a new high-pressure phase around 10 GPa that coexists up to 31 GPa with the LP trigonal phase and up to near 42 GPa with an orthorhombic *I4/mmm* structure also discussed in the two previous high-pressure studies of 1T-$HfSe_2$ quoted above [8,9]. Zhang et al. prefer not to assign any space group to the first emerging phase of 1T-$HfSe_2$, and refer to this polymorph as 'the intermediate high pressure I' without any reference to its symmetry.

In our totally *in-silico* investigation, the focus is on the identification of the first pressure-induced phase of 1T-$HfSe_2$. We discuss the plausibility of the monoclinic and hexagonal structures proposed by Tian et al. [8] and Rahman et al. [9], respectively, and analyze the compatibility of their experimental and theoretical results with each other, with those obtained by Zhang et al. [7], and with our own theoretical predictions. Our extensive DFT calculations of potential candidates reported in other TMDs along with searches performed using evolutionary crystal prediction algorithms [12] lead to two alternative dynamically stable phases with lower enthalpies than the ambient conditions 1T-$HfSe_2$ polymorph at pressures where this first transition was detected. The calculated unit cell parameters, equation of state, and Raman frequencies for our proposed orthorhombic *Immm* candidate are consistent with the experimental data reported so far for $HfSe_2$ and allow us to characterize a convincing structure for the first polymorph into which the 1T-HfSe2 phase transforms under applied hydrostatic pressure. In the following sections, we provide details of our computational simulations (section 2), present and discuss the calculated structural parameters, equations of state, and Raman frequencies of our two lowest enthalpy and previously proposed candidates (section 3), and, finally, summarize our findings suggesting prospective studies (section 4).

2. Computational details

The total energy of the different $HfSe_2$ polymorphs was evaluated by means of periodic DFT electronic structure calculations at selected volumes using the VASP package [13]. The PBE exchange-correlation functional was employed [14]. In order to take into account the van der Waals interactions, a pairwise force field was included through Grimme's DFT-D3 method [15]. A plane-wave basis set with an energy cutoff of 500 eV was used within the PAW scheme [16,17]. Γ-centered Monkhorst−Pack meshes [18] were used to sample the Brillouin zone, where the numbers of subdivisions along each reciprocal lattice vector $\vec{b}_i$ were given by $N_i = \max(1, 90|\vec{b}_i| + 0.5)$. The geometry optimizations were stopped when the forces acting on the nuclei were all less than 10^{-5} eV $Å^{-1}$. Energy-volume points were fitted using numerical and analytical equations of state to obtain the bulk modulus at zero pressure, B_0, its pressure derivative, B_0', and the enthalpy (*H*)–*P* curves. These calculations have been performed with the GIBBS2 code [19]. Simulated X-ray powder diffraction patterns were generated using FULLPROF [20] and experimental plots from external sources were digitized using WebPlotDigitizer [21]. The FINDSYM program was used to analyze the symmetry of the structures [22,23].

The XtalOpt evolutionary algorithm (version 12 [12]) was used to identify low-enthalpy structures for $HfSe_2$ at pressures of 0, 5, 10, 15, and 20 GPa. Searches were performed on $HfSe_2$ structures containing 1–6 formula units in the unit cell, with interatomic distance limit constraints of 2.5 Å on Se–Se contacts and 2.0 Å on both Hf–Se and Hf–Hf contacts. The RandSpg algorithm [24] was used to generate symmetric structures in the first generation and the XtalComp algorithm [25] was used to eliminate duplicate structures. The dynamic stability of the proposed structures was evaluated using the PHONOPY code [26] via the supercell method in which the magnitude of the supercell dimensions was at least 10 Å on each side.

3. Results and discussion

In our search for competitive structures that the 1T-$HfSe_2$ phase (trigonal $P\bar{3}m1$ space group) may transform to under hydrostatic pressure, we have followed two different computational strategies: the first involves local relaxation of a selection of structures found in the same or similar crystal families. A number of structures commonly assumed by MX_2 transition metal dichalcogenides with M = Ti, Zr, Hf and X = O, Se, Te have been considered, and their energy (*E*)-volume (*V*) curves were computed and are plotted in Fig. S1. Eight polymorphs from known TMD compounds were considered in this step, far more than in other recent studies that were restricted to analysing 2 or 3 structures. (see Refs. [7–9]). The second strategy makes use of evolutionary crystal structure searches as implemented in the open-source XtalOpt program package [27]. Searches were conducted at selected pressures between 0 and 20 GPa and the candidate structures within 100 meV/formula unit of the lowest-enthalpy phase at each pressure were reoptimized and incorporated into the *E*-*V* plot. On the basis of these extensive computational results, our aim in this contribution is to provide consistent arguments that lead to the proposal of a convincing polymorph that is an alternative to the *C*2/*m*-T and *P*6$_3$/*mmc* candidates proposed by Tian et al. [8] and Rahman et al. [9], respectively.

To start with, we raise the key question motivating our investigation: what are the evidences supporting the proposal of either the *C*2/*m*-T or the *P*6$_3$/*mmc* structure as the first pressure-induced polymorph of 1T-$HfSe_2$? Since we demonstrate that solid experimental proofs are difficult to find in the otherwise thorough studies of Tian et al. [8] and Rahman et al. [9], new candidates need to be proposed to advance the understanding of the pressure-induced polymorphic sequence of $HfSe_2$. The previously proposed and our current alternative structures are analysed following a four steps strategy: (i) calculation of *H*–*P* curves, (ii) discussion of the dimensionality of the high-pressure phase based on the equations of state (EOS) parameters, and phase transition properties, (iii) experimental and simulated XRD patterns, and (iv) dynamic stability and pressure evolution of experimental and calculated Raman frequencies. For our proposed candidate, we further compare its electronic band structure and emergence of superconductivity with the available observed data. The first two steps provide unequivocal proof that allow us to rule out the structures reported by Tian et al. [8] and Rahman et al. [9] in favour of our alternative candidates. The last three steps serve to check the plausibility of the candidates we found with the lowest enthalpy in the pressure region where 1T- $HfSe_2$ is not thermodynamically stable.

3.1. Thermodynamic considerations: phase stability from ΔH-P calculations

It is clear that, as for any other polymorph, the hexagonal *P*6$_3$/*mmc* structure proposed by Rahman et al. [9] could in principle be observed as metastable even if its enthalpy is not lower than that of other high-pressure structures. However, in order for $HfSe_2$ to transform to this hexagonal polymorph under pressure, basic phase equilibria rules

dictate that the free energy of the $P6_3/mmc$ phase must be lower than that of the starting 1T $P\,\bar{3}\,m1$ polymorph at least at one single (P,T) point within the P/T conditions achieved in experiment. This is mandatory regardless of whether the HP hexagonal phase is considered as a stable or a metastable phase.

Fig. 1 provides the enthalpies of the relevant $HfSe_2$ phases referenced to that of the LP $P\,\bar{3}\,m1$ polymorph. Both in our results of Fig. 1 and in those of Ref. [9], the enthalpy of $P6_3/mmc$ is always at least 0.3 eV/f.u. higher than that of 1T-$HfSe_2$ between 0 and 35 GPa. The very same result was also obtained in the calculations of Tian et al. [8]. Rahman et al. suggest that a poor description of the weak interlayer interactions led to this discrepancy; however, our calculations including Grimme D3 van der Waals corrections still found the enthalpy of the $P6_3/mmc$ structure well above that of $P\,\bar{3}\,m1$. In this discussion (as well as in the experiments in the paper of Rahman et al.), it is very important to bear in mind that the starting point is the LP 1T-$HfSe_2$ phase of $P\,\bar{3}\,m1$ symmetry. Any transition path connecting this LP phase with a hypothetical candidate with higher enthalpy needs to overcome a higher activation barrier for the direct transition than for the reverse one, hindering the transition. As the proposed hexagonal $P6_3/mmc$ HP structure has higher enthalpy than the LP 1T-$HfSe_2$ starting phase, the hypothetical HP hexagonal phase would revert back to the LP 1T-$HfSe_2$ starting phase and would not be observed. In the Supporting Information file, this point is further illustrated by means of schematic energy profiles (Fig. S2) and a subsequent discussion. Though the finite temperature contributions were not calculated, it is unlikely they would be sufficiently large to overcome this difference.

Therefore, it is not clear what would be the driving force for the 1T → $P6_3/mmc$ transition in this pressure range, and how this phase transition is supported by kinetic barriers and the potential metastability of this hexagonal structure as discussed in Ref. [9]. The conclusion from this analysis is that the hexagonal structure cannot be observed at pressures where 1T-$HfSe_2$ is detected to transform to another polymorph, and should therefore be ruled out as a candidate.

Concerning the high-pressure monoclinic $C2/m$–T candidate reported by Tian et al. based upon a comparison of synchrotron X-ray diffraction and Raman experiments, and first-principles simulations [8], there are also some inconsistencies that raise doubts about its plausibility as a convincing high-pressure structure of the room conditions 1T-$HfSe_2$ polymorph. Using the description of the $C2/m$-T unit cell at 30 GPa that Tian et al. provide in the Supporting Information file (Table S2)

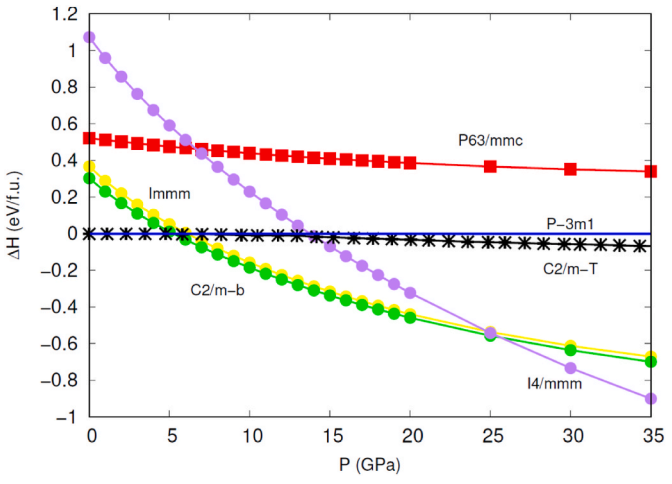

Fig. 1. Calculated ΔH-P curves of six relevant $HfSe_2$ phases discussed in this study and highlighted with purple ($I4/mmm$), red ($P6_3/mmc$), yellow ($Immm$), green ($C2/m$-b), black ($C2/m$-T), and blue ($P\,\bar{3}\,m1$) colors. The enthalpy of the $P\,\bar{3}\,m1$ phase is taken as the reference. Data points and the curve for $C2/m$-T have been extracted from Ref. [8].

[8], we have found that the atomic positions are very similar to the ones of the 1T-$HfSe_2$ polymorph. In fact, the relative enthalpy of $C2/m$-T with respect to the LP 1T-$HfSe_2$ polymorph is within hundredths/thousandths of eV in the relevant 0–10 GPa pressure region according to Fig. S4 of Ref. [8] (see also our Fig. 1). This is the expected result since the $C2/m$-T structure is based on the unit cell reported by Sereika et al. for VSe_2, who report an E-V curve for the monoclinic phase that is almost identical to that of the 1T-VSe_2 structure [11]. Moreover, we have reoptimized the $C2/m$-T structure and used the XtalComp algorithm to determine if the resulting geometry is a duplicate with $P\,\bar{3}\,m1$. Using the default criteria, the two structures were found to be "the same" in the pressure range 0–10 GPa. The resulting similarity of the 1T- $P\,\bar{3}\,m1$ and $C2/m$-T polymorphs is in direct contradiction to the observed change in dimensionality and first order nature of the pressure-induced phase transition of 1T-$HfSe_2$.

The results of our calculations, however (Fig. 1), clearly show two competitive polymorphs with orthorhombic ($Immm$) and monoclinic ($C2/m$-b) symmetry that become lower in enthalpy than both the LP 1T-$P\,\bar{3}\,m1$ and the $C2/m$-T candidate by 6 GPa. These two low enthalpy structures were found thanks to our predictive XtalOpt code [27]. As we mentioned before, thermal effects are not expected to play any meaningful role in the relative stability of these phases at least at the moderate temperatures where the experiments have been performed. In fact, we have used a Debye model [19] that confirms the same order in the Gibbs free energies of these polymorphs. The calculated transition pressures from the 1T-$HfSe_2$ phase to the $Immm$ or $C2/m$-b phases are only 1 GPa greater when the temperature conditions change from static (0 K and zero point vibrational contributions neglected) to 300 K. In summary, all these thermodynamic considerations allow us to replace previous proposals for the first high-pressure phase of 1T-$HfSe_2$ by either the $Immm$ or the $C2/m$-b structures with unit cell parameters and their illustrations in Table S1 and Figs. 2 and 3. At pressure around 25 GPa, the orthorhombic $I4/mmm$ structure shows a lower enthalpy and becomes the thermodynamic stable phase in agreement with all previous studies [7–9].

3.2. *Kinetic considerations: dimensionality of the high-pressure phase*

There are at least three experimental facts pointing towards a change in the structural dimensionality of the first high-pressure phase of 1T-$HfSe_2$: (i) its lower compressibility, (ii) the volume collapse across the phase transition, and (iii) the hysteresis associated with the transition. The new phase should reflect this 2D to 3D change by showing increased atomic coordination numbers and larger distances between nearest neighbors. Concerning point (i), both Tian et al. [8] and Rahman et al. [9] report zero pressure bulk modulus (B_0) values derived from their measured pressure-volume data that are, respectively, 1.6 and 2.4 times higher for the high pressure phase than for the low-pressure 1T-$HfSe_2$ polymorph. This is a clear evidence of the emergence of new stronger covalent bonds replacing weak van der Waals interactions. The same conclusion is drawn as regards point (ii) since in the two previous experimental investigations a decrease in the unit cell volume of about 5% is obtained for the LP-HP transition. This is a signature of a reconstructive first-order phase transition involving a densification of $HfSe_2$ through a more effective atomic packing. Finally, the HP phase was detected in decompression experiments at pressures much lower than the direct transition pressure [7] or even at 0 GPa [8]. The existence of such a wide hysteresis pressure range (point (iii)) implies the existence of a high activation barrier across the transition path that is associated again with a severe bonding reconstruction. In brief, all these observations indicate that the 1T-$HfSe_2$ 2D structure should transform under pressure into a non-laminar polymorph with a 3D chemical bonding network.

However, when we examine the two candidates proposed by Tian et al. and Rahman et al., their atomic organization is still of a laminar 2D

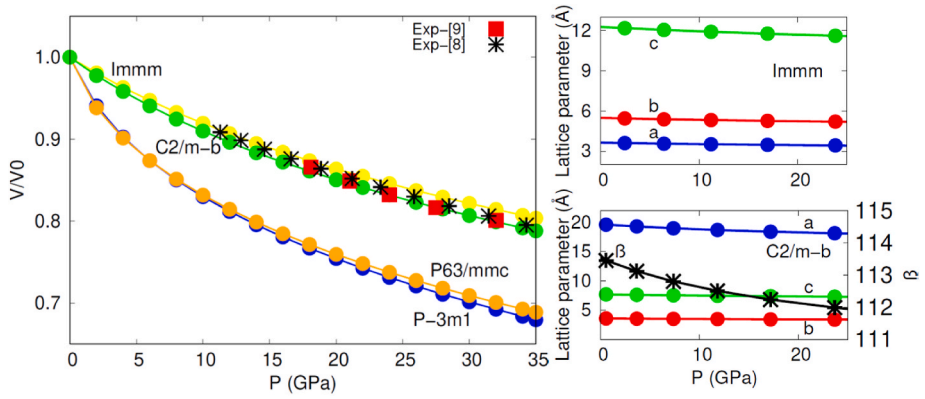

Fig. 2. (Left panel) Pressure evolution of normalized volumes for the four phases involved in the discussion. Red squares and black asterisks stand for the values derived from the experiments reported in Refs. [8,9]. (Right panels) Our calculated lattice parameters of the *Immm* (top) and *C2/m*-b (bottom) phases as a function of pressure.

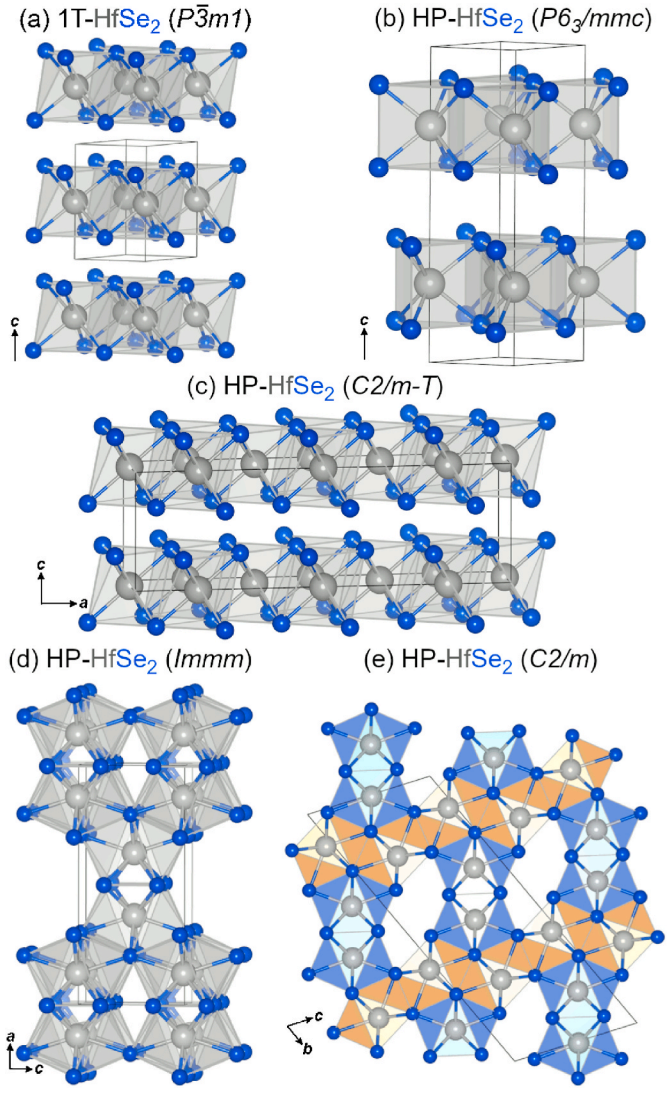

Fig. 3. Polyhedral view of (a) $P\bar{3}m1$ (1T), (b) HP-$P6_3/mmc$, (c) HP-*C2/m*-T, (d) HP-*Immm*, and (e) HP-*C2/m*-b unit cells of $HfSe_2$. Grey and blue balls stand for Hf and Se atoms, respectively.

structure. Rahman et al. explicitly state that their $P6_3/mmc$ candidate keeps a 2D nature to justify a low activation barrier associated with the transition. This result is not consistent with the increase in the B_0 value, the volume collapse and the hysteresis of the transition that they report in their study. On the other hand, Tian et al. claim a 'dimensionality switching' for the transition associated with 1T-$HfSe_2$. Whereas their data clearly provide support to the 3D nature of a second structure (*I4/mmm* symmetry) found at much higher pressures, this is not the case for the first high-pressure phase of 1T-$HfSe_2$. In fact, the Hf and Se coordination numbers they give for their *C2/m*-T candidate still keep the values of the LP 2D polymorph. As we noticed above, the structural and energetic similarities between their *C2/m*-T structure and the one found by Sereika et al. in VSe_2 reveals that this monoclinic polymorph is a 2D laminar structure as recognized in the study of Ref. [11].

The pressure evolution of the normalized volume (V/V_0, V_0 is the corresponding zero pressure volume) of the relevant polymorphs (Fig. 2) and the illustrations of their unit cells (Fig. 3) help us to support the 2D to 3D transformation associated with our candidates. The coordination numbers and representative bond distances (see Table 1) are consistent with this change. The 1T-$HfSe_2$ polymorph is clearly a layered 2D structure with a low zero pressure bulk modulus (B_0) around 30 GPa [6]. Our two candidates possess B_0 values around 90 GPa and display V/V_0–P curves with a much lower slope than that of the $P\bar{3}m1$ polymorph, consistent with a transformation of the weak van der Waals interlayer interactions into covalent bonds. The increase of the *dimensionality* of these structures is also confirmed by their higher coordination numbers compared to the 1-atm 1T-$HfSe_2$ phase. The coordination number (CN)

Table 1
Calculated equation of state (EOS) parameters, coordination numbers (CN), and nearest neighbour distances ($d_{Hf\text{-}Se}$) of $P\bar{3}m1$ (1T) at 0 GPa, and HP-$P6_3/mmc$, HP-*C2/m*-T, HP-*Immm*, and HP-*C2/m*-b at 10 GPa. V_0, B_0, and B_0' values, as obtained in Ref. [9] via fitting to the Murnaghan EOS, for the HP-$P6_3/mmc$ phase, and in Ref. [8] via fitting to the Birch-Murnaghan EOS, for the HP-*C2/m*-T phase, are also included. Superscripts a, b, and c stand for Refs. [6,9], and [8}, respectively.

$HfSe_2$	V_0 (Å^3)	B_0(GPa)	B_0'	CN-Hf	CN–Se	$d_{Hf\text{-}Se}$(Å)
LP-1T- $P\bar{3}m1$	74.96[a]	29.2[a]	7.0[a]	6	3	2.67
HP-$P6_3/mmc$	73.58 65[b]	26.0 86[b]	7.7	6	3	2.63
HP-*C2/m-T*	65.5[c]	98.9[c]	3.6[c]	6	3	2.62
HP-*Immm*	61.43	95.0	6.6	6 + 2	Se1:4 Se2:4	2.65–2.82
HP-*C2/m*-b	62.41	84.3	4.8	Hf1: 6 + 2 Hf2: 6 + 2	Se1: 4 Se2: 5 Se3: 3 Se4: 4	2.64–2.75

of Hf and Se increases from 6 and 3, respectively, in the $P\,\bar{3}\,m1$ polymorph to 6 + 2 and 4 in our *Immm,* and to 6 + 2 and between 3 and 5 in our *C*2/*m*-b candidates. Hf–Se nearest neighbour distances in the HP polymorphs, all calculated at 10 GPa, show increasing values for the structures with higher coordination numbers (see Table 1). For the sake of comparison, the same quantities for the $P6_3/mmc$ and *C*2/*m*-T structures are also included in Table 1 and the unit cells of these structural candidates are plotted in Fig. 3. Detailed information of these structures is provided in Table S1 of the Supporting Information file.

It is also encouraging to see that EOS parameters reported for the high-pressure candidates in Refs. [8,9] are closer to the ones of our two candidates (*Immm* and *C*2/*m*-b) than to a 2D structure like 1T-$HfSe_2$ (see Table 1). This result is apparent in Fig. 2, where we have included {P, V/V_0} data points from the experimental results of Tian et al. and Rahman et al. These points are almost coincident with our DFT calculated *C*2/*m*-b and *Immm* EOS. In contrast, when we examine the hexagonal $P6_3/mmc$ structure, we observe that it is in fact a 2D polymorph as revealed by the similar pressure evolution of its normalized volume when compared with 1T-$HfSe_2$, and by the noticeable separation between its adjacent $HfSe_2$ layers, as is also observed in the $P\,\bar{3}\,m1$ 1T-$HfSe_2$ polymorph (see Fig. 3). We point out that there is a discrepancy between the experimental and our calculated absolute volume values (see Fig. S3), which is roughly uniform and lower than 10% for all the examined phases. This result is not relevant to the discussion of the dimensionality of the LP and HP structures since the indicator of the compressibility of a given phase is the slope of the evolution with pressure of the experimental volumes (B_0 and B_0') rather than the absolute volume values. As we have discussed, the comparison of the experimental results shows much better agreement with either our *Immm* or the *C*2/*m*-b structures than with the $P6_3/mmc$ symmetry or the *C*2/*m*-T candidate that possess so many analogies with the 1T LP phase.

Once again, the scenario is favourable for our alternative candidates. We agree with the authors of Ref. [9] that kinetic effects should be taken into account provided the temperature of the experiments is not high enough to overcome the expected barrier associated with this transition. Moreover, a *pressure delay* should be expected for transitioning into polymorphs that exhibit a partial (larger compared with the 2D character of 1T-$HfSe_2$) or total 3D character. It is known that reconstructive transitions involving transformation of weak van der Waals interactions into covalent bonds with increasing coordination numbers are usually associated with meaningful kinetic barriers [28]. Therefore, the activation energy associated with their emergence from the 1T-$HfSe_2$ structure is expected to be high, which requires either the help of thermal effects to overcome the barrier or overpressure to reduce it. This second possibility is reasonable and would be in-line with the experimental observations of a sluggish phase transition, the coexistence of the LP and HP phases in a wide pressure range, a delay of the onset of the transformation to 10–16 GPa, and the possibility of retaining the high-pressure phase when pressure is decreased down to 0 GPa [7,9]. The calculated phase transition pressures (around 6–7 GPa) of our two 3D structures are consistent with these experimental facts.

In summary, we observe that it is compatible to question the space groups assigned in Refs. [8,9] to the first high-pressure phase of 1T-$HfSe_2$, while "trusting" the volumes obtained from the corresponding experimental XRD diffractograms, which have been used to justify the change from 2D to 3D in the dimensionality of the structures involved in the phase transition.

3.3. Calculated and simulated X-ray diffractograms

The only argument found in Ref. [9] in favour of the hexagonal $P6_3/mmc$ structure is the claimed analogy of its simulated X-ray diffractogram with that obtained experimentally (third and fourth panels from bottom of Fig. 4). However, the quality of high-pressure diffraction data cannot rival results obtained at ambient pressures, and the comparison between the experimental and simulated patterns is, at the very least, not clear, with only 2–3 peaks of $P6_3/mmc$ matching those obtained in experiment.

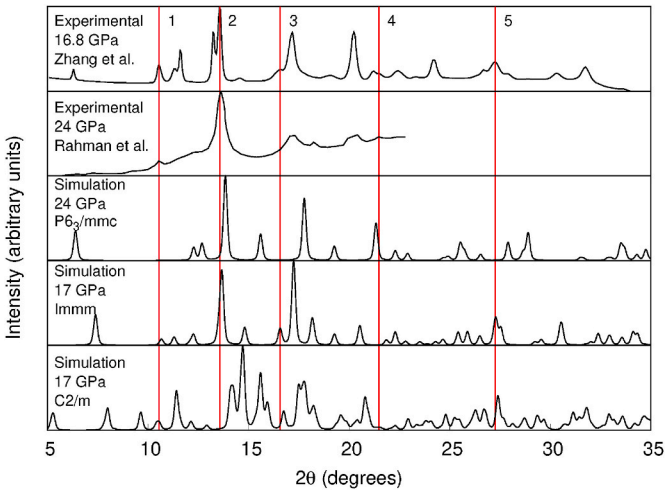

Fig. 4. From top to bottom, the five panels collect patterns from (i) Experimental X-ray data of the so-called Phase-I at 16.8 GPa reported in Ref. [7], (ii) Experimental X-ray data of the proposed $P6_3/mmc$ candidate at 24 GPa reported in Ref. [9], (iii) Simulated X-ray data of the proposed high-pressure $P6_3/mmc$ structure at 24 GPa in Ref. [9], (iv) Simulated X-ray data of our proposed high-pressure *Immm* structure at 17 GPa, and (iv) Simulated X-ray data of our proposed high-pressure *C*2/*m*–b structure at 17 GPa. Vertical red lines highlight the new peaks observed for Phase-I. The wavelength used in the pattern simulation was the same as in the two experiments, 0.6199 Å.

Nevertheless, we have compared this experimental X-ray diffraction pattern obtained for the high-pressure phase in Ref. [9] with those simulated for our *C*2/*m*-b and *Immm* candidates (first and second panels from bottom, respectively, in Fig. 4). Concerning the comparison with our simulated *Immm* pattern, we observe that this candidate does not lead to a worse agreement with the experimental pattern than the hexagonal $P6_3/mmc$ structure used in Ref. [9]. We also notice the existence of some analogies between our (*Immm*) diffractogram and the one of the $P6_3/mmc$ structure proposed by Rahman et al. that could explain the compatibility of the reported volumes for the two structures. We cannot say the same as regards the comparison with our *C*2/*m*-b structure since the most intense peak found in Ref. [9], at around 13–14°, is clearly absent in the simulated pattern of our monoclinic structure. As we noticed above, the quality of the data from Ref. [9] prevents a rigorous analysis and we admit that the comparison cannot be conclusive.

To further investigate this point, we have gone one step further and have also resorted to a comparison with higher quality diffraction data reported in Ref. [7] (top panel in Fig. 4). The comparison is carried out by digitizing the X-ray pattern reported at 16.8 GPa in the Supporting Information file of Ref. [7]. For the peak profile, a pseudo-Voigt function was used with mixing parameter 0.5 and the value of FWHM was set to a constant value of 0.05. We have highlighted with a vertical red line in Fig. 4 each of the five peaks identified in the experiments as belonging to the HP Phase-I. Many of the other peaks belong to the coexisting LP-1T-$HfSe_2$ phase. Notice the analogies between the two experimental patterns in Fig. 4, especially the intense peak identified in the red line 2.

When compared with our *Immm* simulated pattern in the second panel from the bottom, we observe that four out of these five peaks (1, 2, 3, and 5) appear in our pattern in the same position or only very slightly displaced to the right. As regards peak 4, we have also obtained a reflexion at that position although the intensity is almost negligible. Otherwise, most of the peaks of the calculated pattern are compatible with the experimental pattern. Notably, the calculated peak around 17° (one of the most intense peaks in the calculated pattern), matches with an experimental peak attributed in Ref. [7] to the 1T phase exclusively.

Certainly, there is, for example, a relatively intense calculated peak around 7.4° that is absent in the experimental pattern. When comparing calculated and experimental patterns, the presence of sample effects such as preferred orientation that can significantly modify the observed intensities should be taken into account. Overall, the result that we have obtained is that the XRD pattern of our proposed *Immm* structure agrees well with the so-called Phase-I found by Zhang et al. around 11 GPa. Again, we cannot say the same about our proposed *C*2/*m* structure. The intense experimental peak 2 is not present in our simulated pattern and the intense group of peaks calculated between 14 and 16° is not observed in the experimental pattern. Taking into account the compatibility between the experimental X-ray diffractions patterns of Rahman et al. and Tian et al., the conclusion from this analysis is that of our two thermodynamic and kinetically consistent candidates, the *Immm* orthorhombic structure is the only one compatible with the experimental X-ray observations and should be considered as an alternative candidate for the first high-pressure phase of $HfSe_2$.

3.4. Phonon dispersion curves and evolution of Raman frequencies as a function of pressure

To strengthen our proposal, we carried out a verification of the stability of our candidates. To do so, phonon dispersion curves were evaluated for the monoclinic (*C*2/*m*-b) and orthorhombic (*Immm*) candidates. The results are presented in Fig. 5. We observe that both; the monoclinic and the orthorhombic *Immm* structures are dynamically stable at 10 GPa with all positive frequencies in the first Brillouin zone. Both structures fulfill the stability requirements and would be therefore valid candidates for the high-pressure phase of 1T-$HfSe_2$. We also confirmed that the same result is obtained for our alternative *Immm* structure at higher pressures (see Fig. S5).

The comparison of the observed and calculated Raman spectra at different pressures needs a more detailed analysis. We have extracted the experimental frequencies at different pressures from Fig. 2(b) of Ref. [8] and Fig. 3 of Ref. [9] and plotted these data in Fig. 6 following as much as possible the same presentation (lines, points, colors, etc.) as reported in their articles. In our previous study of the LP-1T-$HfSe_2$ polymorph [6], we obtain a very good agreement as regard the evolution of the frequencies of the most representative Raman active modes of this phase. The good agreement remains when the calculated frequencies (blue circles in Fig. 6) are compared here with the experimental values obtained by Tian et al. [8] (orange line) and Rahman et al. [9] (purple squares) for the low pressure phase. Thus, we confirm the consistency between the three different experimental sets of Raman data in LP-1T-$HfSe_2$.

As regards the emerging phase from 1T-$HfSe_2$, the analysis of the

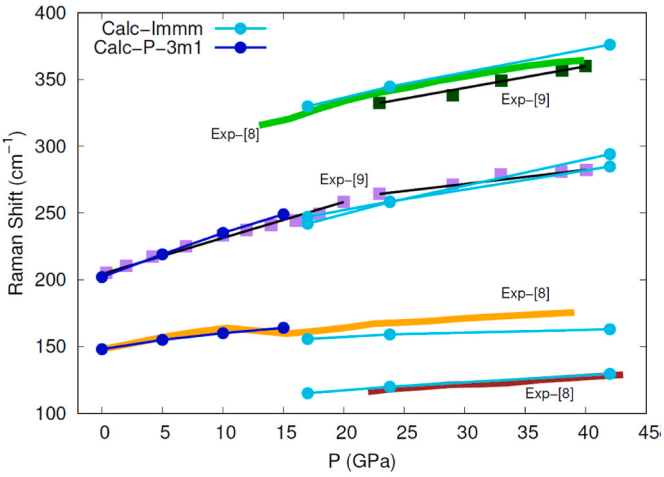

Fig. 6. Pressure evolution of experimental and calculated Raman frequency shifts of $HfSe_2$. Experimental data at low- and high-pressure from Refs. [8,9]. Calculated values of the LP 1T-$P\bar{3}m1$ phase from Ref. [6] and of the HP-*Immm* phase from this study. According to the calculations, the symmetry of the modes of the LP phase is E_g and A_{1g}, and B_{2g}, A_g, B_{3g}, A_g, and A_g for the modes of the HP phase (from the lowest to the highest frequency in each phase).

experimental data of Tian et al. [8] and Rahman et al. [9] reveals the existence of four meaningful new features in the Raman spectra. The first one is common to both experimental investigations and constitutes the most singular peak in the Raman spectrum of the HP phase of 1T-$HfSe_2$. It is a high frequency mode with a positive (sublinear) pressure coefficient that appears around 12 GPa in the experiments of Tian et al. and around 22 GPa in the experiments of Rahman et al. Frequency values lie in the 310-370 cm^{-1} range and are associated with a *N* [8] and a *M6* [9] mode (green line and dark-green squares, respectively, in Fig. 6), but no more information is given for these modes even to explain the meaning of the symbols used in their assignation. A second distinctive feature of the high-pressure Raman spectra appears in the experiments of Rahman et al. in the 260-280 cm^{-1} range. It seems to continue with a lower pressure slope the trend of the A_{1g} mode of the LP-1T-$HfSe_2$ structure (purple squares in Fig. 6). Similarly, Tian et al. found a prolongation of the frequency of the 1T-$HfSe_2$ E_g mode after a small jump to lower frequencies (140-160 cm^{-1}) around 12 GPa (orange line in Fig. 6). Finally, a new low frequency mode at around 120-130 cm^{-1} with a low pressure coefficient in the 15–42 GPa interval is associated by Tian et al. with emerging Se–Se interactions of the HP phase (brown line in Fig. 6).

When these experimental data are compared with our simulated

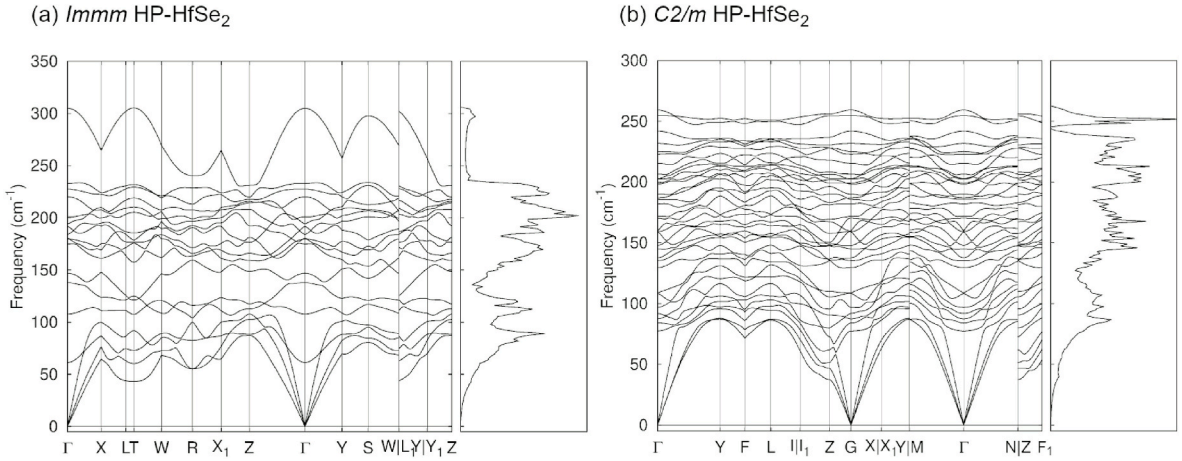

Fig. 5. Calculated phonon dispersion curves along with their projected density of states for *Immm* (a) and *C*2/*m* (b) structures at 10 GPa.

Raman spectra, two unequivocal results are derived. First, neither our *C*2/*m*-b candidate nor the proposed $P6_3/mmc$ [9] and *C*2/*m*-T [8] structures are able to match the trends observed in these experiments. In particular, neither of these structures show frequencies (regardless if they are Raman or IR active or silent) as high as the ones observed experimentally for the high-pressure phase. In the SI file (Table S2), we have collected vibrational frequencies for the *C*2/*m*-b and $P6_3/mmc$ structures at different pressures. The second result is positively eye-catching: Raman frequencies calculated for the *Immm* structure agree qualitatively and quantitatively very well with the experimental values. It is enough to look at the high-pressure region of Fig. 6 to realize that absolute values and trends of the different calculated Raman modes of our *Immm* structure (cyan solid circles and lines) are consistent with the spectra obtained in the experiments of Tian et al. [8] and Rahman et al. [9].

Although the aim of the analysis of the high-pressure Raman spectra of $HfSe_2$ is to assess the coherence of the proposed candidates and not to carry out a general discussion of the mode assignments, we also provide the symmetries of the calculated vibrational modes collected in Fig. 6 (light blue circles) with frequencies at 42 GPa in brackets: B_{2g} (130 cm^{-1}), A_g (163 cm^{-1}), A_g (284 cm^{-1}), B_{3g} (294 cm^{-1}), and A_g (376 cm^{-1}). In addition, the atomic movements associated with the highest and lowest frequency modes of the *Immm* structure are graphically depicted in the SI file (Fig. S4). We notice that in our orthorhombic structure there are up to nine Raman active modes whereas only four are observed in the experiments. Usually, one explanation for this discrepancy is the low intensity of the not observed modes. It is also to be noticed that the lowest frequency mode is below the frequency window of the experimental instrument and that two modes of the *Immm* phase have very similar values and pressure coefficients as illustrated in Fig. 6. Overall, in this subsection we have strengthened the consistency of the calculated observables of the *Immm* candidate with those that were experimentally measured. The agreement with the observed Raman data reported so far cannot be fortuitous and allows us to state that this orthorhombic *Immm* structure represents a plausible alternative for the high-pressure phase of the 1T-$HfSe_2$ polymorph.

3.5. Electronic structure of the high-pressure Immm phase

In the experiments of Tian et al. [8] and Rahman et al. [9], the first high-pressure phase of 1T-$HfSe_2$ shows metallic behaviour and becomes superconducting with a critical temperature (T_c) around 5–6 K in the 24–70 GPa pressure range. Tian et al. remark the almost negligible dependence of T_c with pressure from 40 to 70 GPa. Previous theoretical evaluations of these properties are reduced to the calculations in the $P6_3/mmc$ phase at one specific pressure (24 GPa) reported in Ref. [9].

In order to check whether our alternative high-pressure *Immm phase* is consistent or not with these experimental facts, we have carried out time-demanding calculations aimed at the evaluation of the electronic band structure and the superconducting temperature at different pressures within the range where this phase was found stable.

The VASP program was used to perform calculations of the electron bands, the total and partial density of states for *Immm* $HfSe_2$ at 24 and 42 GPa. Hybrid HSE06 [29] functional was employed. PAW pseudopotentials for both Hf and Se were used, with the Hf valence configuration being treated as $6s^2\ 5d^2$ and the Se valence configuration being $4s^2\ 4p^4$. The *k*-point grid used was $8 \times 8 \times 8$ for the electron bands and $10 \times 10 \times 10$ for the density of states with a plane-wave energy cutoff of 500 eV. The VASPKIT [30] program was used to process VASP output. *k*-points paths for band calculations were taken from Ref. [31]. Fig. 7 illustrates our results at 24 GPa.

The electronic density of states (DOS) of the valence band reveals that it is predominately formed by Se *p* states and Hf states. Conduction band is predominately formed by Hf *d* states with minor contributions of other orbitals. Overlap between both bands consists in a low DOS region extended for about 2 eV before Fermi Level and to 0.5 eV above it with approximately equal contributions of Hf *d* and Se *p* states. In the band diagram this corresponds to one valence band traversing the Fermi level at some directions of the Brillouin zone (at the left in the diagram) and one conduction band with its bottom below that level in other directions (at the right in the diagram). This overlapping low DOS valence-conduction bands is a characteristic feature of semimetals and is compatible with the metal character but the low conductivity values found experimentally [8,9]. Electronic structure studies carried out at higher pressure (42 GPa) do not show any qualitative change.

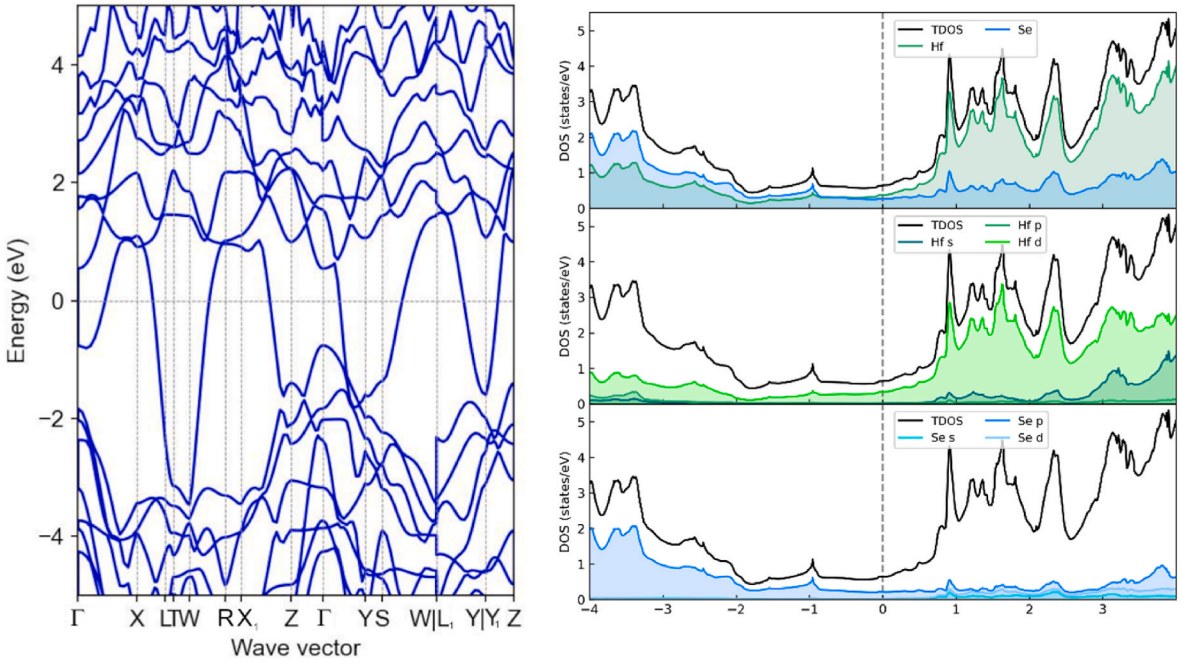

Fig. 7. (Left) DFT-based calculations of the band structure of *Immm* $HfSe_2$ at 24 GPa within HSE06 hybrid functional. (Right) Total and partial electronic density of states (DOS) for Hf and Se (upper panel), orbital decomposition for Hf (middle panel) and Se (bottom panel) at 24 GPa.

The Quantum Espresso program [32,33] was used to perform calculations of the electron-phonon coupling (EPC) for *Immm* $HfSe_2$ at 25 and 40 GPa. PAW pseudopotentials for both Hf and Se were used, with the Hf valence configuration being treated as $5s^2\ 5p^6\ 6s^2\ 5d^2$ and the Se valence configuration being $4s^2\ 4p^4$. The *k*-point grid used was 16 × 16 × 16 with a plane-wave energy cutoff of 60 Ry. The density functional perturbation theory implementation was used to perform the phonon calculations, with a 4 × 4 × 4 *q*-mesh used for evaluation of the EPC elements. The convergence of the EPC parameter λ was tested with a range of Gaussian broadenings ranging from 0.005 to 0.05, with a final selection of 0.025 Ry.

Prompted by the reports of pressure-induced metallicity and a superconducting transition in $HfSe_2$, as well as the demonstrated metallicity of the proposed *Immm* phase using the HSE06 functional, we investigated the possible superconducting transition for *Immm* $HfSe_2$. For conventional, phonon-mediated superconductors, the Allen-Dynes modified McMillan equation (Eq. 1) [34], suitable for estimating T_c for conventional superconductors in the limit $\lambda < 1.0$, was then used to calculate an estimated T_c with the μ^* parameter varied from 0.1 to 0.15:

$$T_c = \frac{\omega_{ln}}{1.2}\exp\left[-\frac{1.04(1+\lambda)}{-\mu^*(1+0.62\lambda)}\right] \quad (1)$$

Here, ω_{ln} is the logarithmic average phonon frequency and μ* the Coulombic repulsion parameter, which is set to vary from 0.1 to 0.15. We thus calculated the electron-phonon coupling parameter λ using the Quantum Espresso software package, finding $\lambda = 0.32$ at both 25 and 40 GPa of pressure. Fig. 8 illustrates our results at 25 GPa. This relatively weak electron-phonon coupling yields a modest estimate for T_c of 0.17–0.01 K (μ* = 0.1–0.15), but nevertheless we find that experimental observation of a superconducting transition might be expected for this compound.

4. Conclusions

In summary, we believe that enthalpy and stability criteria, EOS parameters, and simulated X-ray diffraction patterns and Raman spectra provide a reasonable explanation to support that the experimentally observed high-pressure phase of $HfSe_2$ can be a structure with *Immm* symmetry. Since the *C*2/*m*-b polymorph is competitive in terms of the enthalpy, a lower energy barrier is expected for the transition to the orthorhombic than to the monoclinic structure. The proposed *Immm* candidate follows very well the experimentally reported *P*–*V* data, fulfills the requisites for a broad hysteresis pressure range associated with the observed phase transition, and its simulated X-ray diffraction pattern is compatible with the new peaks appearing in X-ray diffraction patterns observed after applying pressure to the 1T-$HfSe_2$ polymorph. Moreover, the simulated Raman spectra of the orthorhombic *Immm* structure agrees very well with the values and pressure trends of the frequencies observed in the experimental studies of Tian et al. [8] and Rahman et al. [9].

As discussed in the previous experimental works repeatedly cited in this paper [7–9], changes in the structural stability of the $HfSe_2$ polymorph are clear first signs or precursors of new electronic phenomena (*i.e.* metallization and superconductivity) that we have also found consistent with the new *Immm* structure found in our study. The experimental confirmation of this orthorhombic structure at high-pressure is attractive not only for $HfSe_2$, but is also of relevance for other compounds and TMD materials exhibiting the 1T-$P\bar{3}m1$ structure at lower pressures. To the best of our knowledge, the symmetry of the high-pressure phase that emerged after a first-order transition from a $P\bar{3}m1$ structure has not been unequivocally reported so far. We notice that this LP trigonal structure is the archetypical polymorph of CdI_2, whose crystal chemistry has been investigated in detail for a number of compounds [35] being UTe_2 the only one crystalizing with the *Immm* symmetry. During the review process, two investigations, one experimental

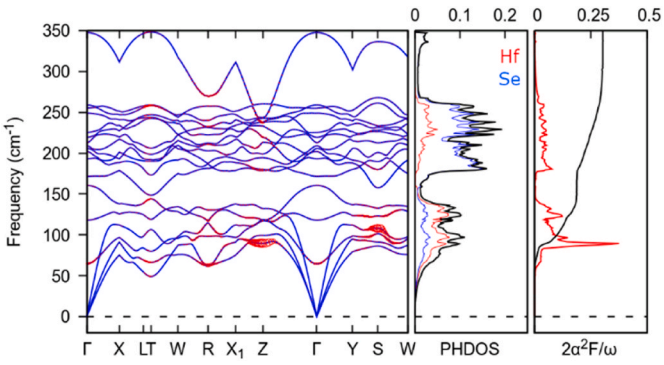

Fig. 8. (Left panel) Phonon band structure of *Immm* $HfSe_2$ (25 GPa). The contribution to the electron-phonon coupling from each phonon mode at wavevector *q* with frequency *ν* in the band structure is represented by an overlaid red circle. (Center panel) Total phonon density of states (black) with projected contributions from Hf (red) and Se (blue). (Right panel) Eliashberg spectral function $2\alpha^2F(\omega)/\omega$ (red) and the integrated electron-phonon coupling λ (black) indicates that the primary contributions to λ occur for low-frequency phonon modes. In particular, the strongest contributions are around the Z and S points.

[36] and the other a combined experimental and theoretical work [37], have been published reporting the same *Immm* structure as the one we propose here, but for the high-pressure phase of another member of this crystal family (1T-HfS_2).

Credit author statement

Katerina P. Hilleke: Methodology, Computational Analysis and Modelling, Graphics, Writing – review & editing. Ruth Franco: Computational Analysis and Modelling, Graphics, Writing – review & editing. Pilar Pertierra: Computational Analysis and Modelling, Graphics, Writing – review & editing. Miguel Á. Salvadó: Computational Analysis and Modelling, Graphics, Writing – review & editing. Eva Zurek: Methodology, Computational Analysis and Modelling, Writing – review & editing. J. Manuel Recio: Conceptualization, Data analysis and Modelling, Writing – review & editing.

Declaration of competing interest

The authors declare that they have no known competing financial interests or personal relationships that could have appeared to influence the work reported in this paper.

Data availability

Data will be made available on request.

Acknowledgements

R.F, P.P, M.A.S., and J.M.R. acknowledge financial support from the Spanish National Research Agency (AEI) through projects PID2021-122588-NB-C21 and RED2018-102612-T, and Principado de Asturias (FICYT) and FEDER under project AYUD/2021/51036. MALTA-Consolider supercomputing center is gratefully acknowledged for computational facilities. J.M.R is grateful to the Spanish Government and the Fulbright Commission for a grant (PRX21/0065) to support his stay at the University at Buffalo-SUNY. K.H. is thankful to the U.S. Department of Energy, National Nuclear Security Administration, through the Capital-DOE Alliance Center under Cooperative Agreement DE-NA0003975 for financial support. Calculations were performed at the Center for Computational Research at SUNY Buffalo (http://hdl.handle.net/10477/79221).

Appendix A. Supplementary data

Supplementary data to this article can be found online at https://doi.org/10.1016/j.mtphys.2023.101152.

References

[1] D. Voiry, A. Mohite, M. Chhowalla, Phase engineering of transition metal dichalcogenides, Chem. Soc. Rev. 44 (2015) 2702–2712, https://doi.org/10.1039/C5CS00151J.

[2] G. Fiori, F. Bonaccorso, G. Iannaccone, T. Palacios, D. Neumaier, A. Seabaugh, S. K. Banerjee, L. Colombo, Electronics based on two-dimensional materials, Nat. Nanotechnol. 9 (2014) 768–779, https://doi.org/10.1038/nnano.2014.207.

[3] M.J. Large, S.P. Ogilvie, M. Meloni, A. Amorim Graf, G. Fratta, J. Salvage, A.A. K. King, A.B. Dalton, Functional liquid structures by emulsification of graphene and other two-dimensional nanomaterials, Nanoscale 10 (2018) 1582–1586, https://doi.org/10.1039/C7NR05568D.

[4] S. García-Dalí, J.I. Paredes, J.M. Munuera, S. Villar-Rodil, A. Adawy, A. Martínez-Alonso, J.M.D. Tascón, Aqueous cathodic exfoliation strategy toward solution-processable and phase-preserved MoS2 nanosheets for energy storage and catalytic applications, ACS Appl. Mater. Interfaces 11 (2019) 36991–37003, https://doi.org/10.1021/acsami.9b13484.

[5] G. Zhang, Y.-W. Zhang, Thermoelectric properties of two-dimensional transition metal dichalcogenides, J. Mater. Chem. C 5 (2017) 7684–7698, https://doi.org/10.1039/C7TC01088E.

[6] A. Andrada-Chacón, Á. Morales-García, M.A. Salvadó, P. Pertierra, R. Franco, G. Garbarino, M. Taravillo, J.A. Barreda-Argüeso, J. González, V.G. Baonza, J. M. Recio, J. Sánchez-Benítez, Pressure-driven metallization in hafnium diselenide, Inorg. Chem. 60 (2021) 1746–1754, https://doi.org/10.1021/acs.inorgchem.0c03223.

[7] X. Zhang, B. Liu, S. Liu, J. Li, R. Liu, P. Wang, Q. Dong, S. Li, H. Tian, Q. Li, B. Liu, Semiconductor-to-metal transition in HfSe2 under high pressure, J. Alloys Compd. 867 (2021): 158923, https://doi.org/10.1016/j.jallcom.2021.158923.

[8] C. Tian, Y. Gao, F. Tian, X. Wang, Z. Zhang, D. Duan, X. Huang, T. Cui, Dimensionality switching and superconductivity transition in dense 1T-HfSe2, Phys. Rev. B 105 (2022): L180506, 1-6, https://link.aps.org/doi/10.1103/PhysRevB.105.L180506.

[9] S. Rahman, H. Saqib, X. Liang, D. Errandonea, A.S. Resta, A. Molina-Sanchez, G. Gao, L. Wang, Y. Tian, H.-K. Mao, Pressure-induced metallization and robust superconductivity in pristine 1T-HfSe2, Mater, Today Phys 25 (2022): 100698, https://doi.org/10.1016/j.mtphys.2022.100698.

[10] Y.I. Joe, X.M. Chen, P. Ghaemi, K.D. Finkelstein, G.A. de la Peña, Y. Gan, J.C. T. Lee, S. Yuan, J. Geck, G.J. MacDougall, T.C. Chiang, S.L. Cooper, E. Fradkin, P. Abbamonte, Emergence of charge density wave domain walls above the superconducting dome in 1T-TiSe2, Nat. Phys. 10 (2014) 421–425, https://doi.org/10.1038/nphys2935.

[11] R. Sereika, Ch Park, C. Kenney-Benson, S. Bandaru, N.J. English, Q. Yin, H. Lei, N. Chen, Ch-J. Sun, S.M. Heald, J. Ren, J. Chang, Y. Ding, H.-k. Mao, Novel superstructure-phase two-dimensional material 1T-VSe2 at high pressure, J. Phys. Chem. Lett. 11 (2020) 380–386, https://doi.org/10.1021/acs.jpclett.9b03247.

[12] P. Avery, C. Toher, S. Curtarolo, E. Zurek, XtalOpt Version r12: an open-source evolutionary algorithm for crystal structure prediction, Comput. Phys. Commun. 237 (2019) 274–275, https://doi.org/10.1016/j.cpc.2018.11.016.

[13] G. Kresse, J. Furthmuller, Efficient iterative schemes for ab initio total-energy calculations using a plane-wave basis set, Phys. Rev. B 54 (1996) 11169–11186, https://doi.org/10.1103/PhysRevB.54.11169.

[14] J.P. Perdew, K. Burke, M. Ernzerhof, Generalized gradient approximation made simple, Phys. Rev. Lett. 77 (1996) 3865–3868, https://doi.org/10.1103/PhysRevLett.77.3865.

[15] S. Grimme, J. Antony, S. Ehrlich, H. Krieg, A consistent and accurate ab initio parametrization of density functional dispersion correction (DFT-D) for the 94 Elements H-Pu, J. Chem. Phys. 132 (2010): 154104, https://doi.org/10.1063/1.3382344.

[16] P.E. Blochl, Projector augmented-wave method, Phys. Rev. B 50 (1994) 17953–17979, https://doi.org/10.1103/PhysRevB.50.17953.

[17] G. Kresse, D. Joubert, From ultrasoft pseudopotentials to the projector augmented-wave method, Phys. Rev. B 59 (1999) 1758–1775, https://doi.org/10.1103/PhysRevB.59.1758.

[18] H.J. Monkhorst, J.D. Pack, Special points for brillouin-zone integrations, Phys. Rev. B 13 (1976) 5188–5192, https://doi.org/10.1103/PhysRevB.13.5188.

[19] A. Otero-de-la-Roza, D. Abbasi-Pérez, V. Luaña, Gibbs2: a new version of the quasi-harmonic model code. II. Models for solid-state thermodynamics, features and implementation, Comput. Phys. Commun. 182 (2011) 2232–2248, https://doi.org/10.1016/j.cpc.2011.05.009.

[20] J. Rodriguez-Carvajal, FULLPROF: a program for rietveld refinement and pattern matching analysis, in: Abstracts of the Satellite Meeting on Powder Diffraction of the XV Congress of the IUCr, Toulouse, France, 1990, p. 127. https://www.ill.eu/sites/fullprof.

[21] A. Rohatgi, WebPlotDigitizer 4.5 and 4.6. https://automeris.io/WebPlotDigitizer. (Accessed 21 February 2023).

[22] H.T. Stokes, D.M. Hatch, FINDSYM: program for identifying the space-group symmetry of a crystal, J. Appl. Crystallogr. 38 (2005) 237–238, https://doi.org/10.1107/S0021889804031528.

[23] Stokes, H. T.; Hatch, D. M.; Campbell, B. J., FINDSYM, ISOTROPY Software Suite, (iso.byu.edu).

[24] P. Avery, E. Zurek, RandSpg: an open-source program for generating atomistic crystal structures with specific space groups, Comput. Phys. Commun. 213 (2017) 208–216, https://doi.org/10.1016/j.cpc.2016.12.005.

[25] D.C. Lonie, E. Zurek, Identifying duplicate crystal structures: XtalComp, an open-source solution, Comput. Phys. Commun. 183 (2012) 690–697, https://doi.org/10.1016/j.cpc.2011.11.007.

[26] A. Togo, I. Tanaka, First principles phonon calculations in materials science, Scripta Mater. 108 (2015) 1–5. https://doi-org.gate.lib.buffalo.edu/10.1016/j.scriptamat.2015.07.021.

[27] Z. Falls, P. Avery, X. Wang, K.P. Hilleke, E. Zurek, The XtalOpt evolutionary algorithm for crystal structure prediction, J. Phys. Chem. C 125 (2021) 1601–1620, https://doi.org/10.1021/acs.jpcc.0c09531.

[28] Flórez, M.; Recio, J. M., Mechanisms of pressure-induced phase transitions, in: Recio, J. M.; Menéndez, J. M.; Otero-de-la-Roza, A. (Eds.), An Introduction to High-Pressure Science and Technology. CRC, Boca Raton, FL: pp. 51-74. https://doi.org/10.1201/b19417.

[29] A.V. Krukau, O.A. Vydrov, A.F. Izmaylov, G.E. Scuseria, Influence of the exchange screening parameter on the performance of screened hybrid functionals, J. Chem. Phys. 125 (2006): 224106, https://doi.org/10.1063/1.2404663.

[30] V. Wang, N. Xu, J.C. Liu, G. Tang, W.T. Geng, VASPKIT: a user-friendly interface facilitating high-throughput computing and analysis using VASP code, Comput. Phys. Commun. 267 (2021): 108033, https://doi.org/10.1016/j.cpc.2021.108033.

[31] W. Setyawan, S. Curtarolo, High-throughput electronic band structure calculations: challenges and tools, Comput. Mater. Sci. 49 (2010) 299–312, https://doi.org/10.1016/j.commatsci.2010.05.010.

[32] P. Giannozzi, et al., Quantum espresso: a modular and open-source software project for quantum simulations of materials, J. Phys. Condens. Matter 21 (2009): 399502, https://doi.org/10.1088/0953-8984/21/39/395502.

[33] P. Giannozzi, et al., Advanced capabilities for materials modelling with Quantum Espresso, J. Phys. Condens. Matter 29 (2017): 465901, https://doi.org/10.1088/1361–648X/aa8f79.

[34] P.B. Allen, R.C. Dynes, Transition temperature of strong-coupled superconductors reanalyzed, Phys. Rev. B 12 (1975) 905, https://doi.org/10.1103/physrevb.12.905.

[35] N.V. Podberezskaya, S.A. Magarill, N.V. Pervukhina, S.V. Borisov, Crystal chemistry of dichalcogenides MX2, J. Struct. Chem. 42 (2001) 654–681, https://doi.org/10.1023/A:1013106329156.

[36] W. Zhong, W. Deng, F. Hong, B. Yue, Structural and electronic phase transition in the van der Waals crystal HfS2 under high pressure, Phys. Rev. B 107 (2023): 134118, https://doi.org/10.1103/PhysRevB.107.134118.

[37] S. Rahman, L. Wang, H. Saqib, D. Errandonea, L. Yang, Y. Zhao, Y. Zhuang, G. Gao, L. Wang, Y. Tian, Metallization and superconductivity with Tc > 12 K in transition metal dichalcogenide HfS2 under pressure, Mater, Today Phys 34 (2023): 101091, https://doi.org/10.1016/j.mtphys.2023.101091.